Rare isotope formation in complete fusion and multinucleon transfer reactions in collisions of ^{48}Ca + ^{248}Cm near Coulomb barrier energies

Peng-Hui Chen,[1,2,*] Fei Niu,[3] Xin-Xing Xu,[2] Zu-Xing Yang,[4] Xiang-Hua Zeng,[5] and Zhao-Qing Feng[3,†]

[1]*School of Physics Science and Technology, Yangzhou University, Yangzhou 225009, China*
[2]*Institute of Modern Physics, Chinese Academy of Sciences, Lanzhou 730000, China*
[3]*School of Physics and Optoelectronics, South China University of Technology, Guangzhou 510641, China*
[4]*RIKEN Nishina Center, Wako, Saitama 351-0198, Japan*
[5]*College of Electrical, Power and Energy Engineering, Yangzhou University, Yangzhou 225009, China*

(Received 25 January 2022; accepted 2 March 2022; published 11 March 2022)

Within the framework of the dinuclear system model, the reaction mechanisms for synthesizing target-like isotopes from Bk to compound nuclei Lv are thoroughly investigated in complete and incomplete fusion reactions of ^{48}Ca + ^{248}Cm near Coulomb barrier energies. The production cross section of ^{292,293}Lv as a function of excitation energy in fusion-evaporation reactions and target-like isotopic yields in multinucleon transfer reactions are evaluated, and a statistical approach is used to describe the decay process of excited nuclei. The available experimental data can be reproduced reasonably well with the model. The products of all possible formed isotopes in the dynamical preequilibrium process for collision partners at incident energy $E_{\rm lab} = 5.5$ MeV/nucleon are exported, systematically. It was found that the quasifission fragments are dominant in the yields. The optimal pathway from the target to compound nuclei shows up along the valley of potential surface energy. The effective impact parameter of two colliding partners leading to compound nuclei is selected from head-on collision to semicentral collision with $L = 52\hbar$. The timescale boundary between complete fusion and multinucleon transfer reactions is about 5.7×10^{-21} s with effective impact parameters. The synthesis cross sections of unknown neutron-rich actinides from Bk to Rf have been predicted to be around several nanobarns.

DOI: 10.1103/PhysRevC.105.034610

I. INTRODUCTION

To find the limits of the nuclear landscape, theoretical and experimental nuclear physicists devote themselves to exploring the synthesis of exotic nuclei and superheavy elements (SHEs) toward drip lines and islands of stability via heavy-ion collisions. For producing unknown superheavy elements, fusion-evaporation reactions have been widely used in different laboratories all over the world. In reactions of actinides with a double magic ^{48}Ca beam at the Flerov Laboratory of Nuclear Reactions (FLNR, Dubna) [1,2], the synthesis of SHEs with atomic number Z up to 118 has been claimed. At Gesellschaft für Schwerionenforschung (GSI), the production of superheavy elements with $Z = 107$–112, 114–117 has been identified [3,4]. The production of new element nihonium ($Z = 113$) in collisions of ^{70}Zn + ^{209}Bi has been observed at RIKEN [5]. The element flerovium ($Z = 114$) has been synthesized at Lawrence Berkeley National Laboratory (LBNL, Berkeley) [6]. The group SHE has synthesized superheavy isotopes dubnium ($Z = 105$), bohrium ($Z = 107$), and darmstadtium ($Z = 110$) at the Institute of Modern Physics (IMP, Lanzhou) [7–9]. To produce exotic transuranium isotopes, multinucleon transfer (MNT) reactions are proposed to perform experiments with radioactive beams in laboratories. They have the advantage that products are formed with wide mass region owing to broad excitation functions in the MNT products. The complete fusion reactions between two heavy partners at energies near the Coulomb barrier are strongly damped by competing incomplete fusion reactions (quasifission and deep-inelastic reactions). Therefore, more insightful theoretical and experimental studies of the reaction mechanisms are required to make a precise prediction for the probability of compound nuclei and MNT products in such reactions.

Quasifission and deep-inelastic heavy-ion collisions have been extensively investigated in experiments since the 1970s, in which MNT reactions had been proposed to synthesize superheavy elements initially. However, new neutron-rich projectile-like fragments and proton-rich actinide nuclei were observed in laboratories [10–16]. In particular, isospin asymmetric collisions may provide valuable information on the production mechanism of exotic heavy nuclei. In laboratories worldwide, the reactions of ^{136}Xe + ^{208}Pb [17,18], ^{136}Xe + ^{198}Pt [19], ^{156,160}Gd + ^{186}W [20], and ^{238}U + ^{232}Th [21] have been performed to create unknown neutron-rich heavy nuclei near the neutron shell $N = 126$, to understand the origin of heavy elements in nuclear astrophysics.

Following the motivation for predicting exotic heavy and superheavy nuclei, several models have been developed, such as the dynamical model based on multidimensional Langevin

*Corresponding author: chenpenghui@yzu.edu.cn
†Corresponding author: fengzhq@scut.edu.cn

equations [22,23], the time-dependent Hartree-Fock (TDHF) approach [24–27], the GRAZING model [28,29], the improved quantum molecular dynamics (ImQMD) model [30,31], the Langevin-type dynamical equations [32,33], the dinuclear system (DNS) model [34–39], etc. Some interesting issues of synthesis mechanism, total kinetic energy spectra, and structure effect have been stressed. There are still some open problems for strongly damped reactions, for example the mechanism of preequilibrium particles emission, the stiffness of the nuclear surface during the nucleon transfer process, the mass limitation of new isotopes with stable heavy targets nuclides, etc.

The three laboratories FLNR [40], GSI [41], and RIKEN [42] obtained cross-section excitation functions of 3n, 4n evaporation channels for production of superheavy element $Z = 116$ in ^{48}Ca induced reactions with ^{248}Cm targets, early or late, respectively. In the experiments of synthesizing superheavy nuclei ($Z = 116$) with $^{48}\mathrm{Ca} + ^{248}\mathrm{Cm}$ [43–47], massive independent yields of target-like fragments have been observed, especially the new heavy isotopes involved. The production cross section of all formed products brings us an opportunity to investigate the interplay between equilibrium and dissipation for low energy heavy-ion collisions as well as decay properties of excited SHEs. So it attracts our interest to explore nuclear dynamics of reaction mechanisms in complete and incomplete fusion in terms of evolution time and dissipation energy.

In this work, ^{48}Ca induced complete and incomplete fusion reactions with ^{248}Cm are calculated with the DNS model. The aim of this paper is to study the dynamics of the synthesis cross sections of nuclides in the complete and incomplete fusion of ^{248}Cm with ^{48}Ca projectile. The article is organized as follows: In Sec. II we give a brief description of the DNS model. Calculated results and discussions are presented in Sec. III. A summary is given in Sec. IV.

II. MODEL DESCRIPTION

The dynamical complete and incomplete fusion mechanisms are described as a diffusion process, in which the resulting distribution probability is obtained by solving a set of master equations numerically in the potential energy surface of the DNS. The time evolution of the distribution probability $P(Z_1, N_1, E_1, \beta, t)$ for fragment 1 with proton number Z_1, neutron number N_1, excitation energy E_1, and quadrupole deformation β is described by the following master equations:

$$\begin{aligned}\frac{dP(Z_1,N_1,E_1,\beta,t)}{dt} &= \sum_{Z_1'} W_{Z_1,N_1,\beta;Z_1',N_1,\beta'}(t)\big[d_{Z_1,N_1}P(Z_1',N_1,E_1',\beta',t) \\ &\quad - d_{Z_1',N_1}P(Z_1,N_1,E_1,\beta,t)\big] \\ &\quad + \sum_{N_1'} W_{Z_1,N_1,\beta;Z_1,N_1',\beta}(t)\big[d_{Z_1,N_1}P(Z_1,N_1',E_1',\beta',t) \\ &\quad - d_{Z_1,N_1'}P(Z_1,N_1,E_1,\beta,t)\big]. \end{aligned} \tag{1}$$

$W_{Z_1,N_1,\beta;Z_1',N_1,\beta}$ ($W_{Z_1,N_1,\beta,;Z_1,N_1',\beta}$) is the mean transition probability from the channel (Z_1, N_1, E_1, β) to (Z_1', N_1, E_1', β) [or (Z_1, N_1, E_1, β) to (Z_1, N_1', E_1', β)], and d_{Z_1,Z_1} denotes the microscopic dimension corresponding to the macroscopic state (Z_1, N_1, E_1). J is the entrance angular momentum. The sum is taken over all possible proton and neutron numbers that fragment (Z_1', N_1') may take, but only one nucleon transfer is considered in the model with the relations $Z_1' = Z_1 \pm 1$ and $N_1' = N_1 \pm 1$. The excitation energy E_1 for fragment (Z_1, N_1) is evaluated by $E_1 = \varepsilon^*(t = \tau_{int})A_1/A$, where $A_1 = Z_1 + N_1$ and the A is mass number of compound nuclei. The interaction time τ_{int} in the dissipative process of two colliding nuclei is dependent on the incident energy $E_{\mathrm{c.m.}}$, B, and J, which are calculated by the deflection function method [48]. The energy dissipated into the DNS increases exponentially [49].

The motion of nucleons in the interacting potential is governed by the single-particle Hamiltonian. The excited DNS opens a valence space in which the valence nucleons have a symmetrical distribution around the Fermi surface. Only the particles at the states within the valence space are active for nucleon transfer. The transition probability is related to the local excitation energy, which is microscopically derived from the interaction potential in valence space as

$$\begin{aligned} W_{Z_1,N_1,\beta;Z_1',N_1,\beta'} &= \frac{\tau_{\mathrm{mem}}(Z_1,N_1,\beta,E_1;Z_1',N_1,\beta',E_1')}{d_{Z_1,N_1}d_{Z_1',N_1}\hbar^2} \\ &\quad \times \sum_{ii'} |\langle Z_1',N_1,E_1',i'|V|Z_1,N_1,E_1,i\rangle|^2. \end{aligned} \tag{2}$$

The memory time τ_{mem} and interaction element V can be seen in Ref. [50]. A similar approach is used for the neutron transition coefficient. The averages on these quantities are performed in the valence space [51].

The local excitation energy is determined by the dissipation energy from the relative motion and the potential energy surface of the DNS as

$$\varepsilon^*(t) = E^{\mathrm{diss}}(t) - [U(\{\alpha\}) - U(\{\alpha_{\mathrm{EN}}\})]. \tag{3}$$

The entrance channel quantities $\{\alpha_{\mathrm{EN}}\}$ include the proton and neutron numbers, quadrupole deformation parameters, and orientation angles, Z_{P}, N_{P}, Z_{T}, N_{T}, R, β_{P}, β_{T}, θ_{P}, θ_{T}, for projectile and target nuclei with the subscripts P and T, respectively. The symbol α denotes the sign of the quantities Z_1, N_1, Z_2, N_2, R, β_1, β_2, θ_1, θ_2 for projectile-like fragments and target-like fragments. Here we set the collision orientations to tip-tip configuration in the following calculations.

The energy dissipated into the DNS is expressed as

$$\begin{aligned} E^{\mathrm{diss}}(t) &= E_{\mathrm{c.m.}} - B - E_{\mathrm{rad}}(J,0)\exp(-t/\tau_r) \\ &\quad - \frac{\langle J(t)\rangle[\langle J(t)\rangle + 1]\hbar^2}{2\zeta} \end{aligned} \tag{4}$$

with

$$\langle J(t)\rangle = J_{\mathrm{st}} + (J_i - J_{\mathrm{st}})\exp(-t/\tau_J). \tag{5}$$

Here $E_{\mathrm{c.m.}}$ and B are the center of mass energy and Coulomb barrier, respectively. The relaxation time of the radial motion is $\tau_r = 5 \times 10^{-22}$ s and the radial energy at the initial state

is $E_{\rm rad}(J,0) = E_{\rm c.m.} - B - J_i(J_i+1)\hbar^2/(2\zeta_{\rm rel})$. The angular momentum at the sticking limit is $J_{st} = J_i\zeta_{\rm rel}/\zeta_{\rm tot}$ and the relaxation time of angular momentum is $\tau_J = 15\times10^{-22}$ s. $\zeta_{\rm rel}$ and $\zeta_{\rm tot}$ are the relative and total moments of inertia of the DNS, respectively, where the quadrupole deformations are implemented. The initial angular momentum is $J_i = J$ in the following.

The potential energy surface (PES) of the DNS is evaluated by

$$U_{\rm dr}(t) = B(Z_1,N_1) + B(Z_2,N_2) - B(Z,N) + V(Z_1,N_1,\beta'_{\rm T}(t),Z_2,N_2,\beta'_{\rm P}(t)) + V_{\rm def}(t) \quad (6)$$

with

$$V_{\rm def}(t) = \frac{1}{2}C_1[\beta_1-\beta'_{\rm T}(t)]^2 + \frac{1}{2}C_2[\beta_2-\beta'_{\rm P}(t)]^2,$$
$$C_i = (\lambda-1)(\lambda+2)R_{\rm N}^2\sigma - \frac{3}{2\pi}\frac{Z^2e^2}{R_{\rm N}(2\lambda+1)}. \quad (7)$$

The interaction potential $V(Z_1,N_1,\beta'_{\rm T}(t),Z_2,N_2,\beta'_{\rm P}(t))$ is composed of Coulomb and nuclear potentials which are calculated by the Wong formula and the double folding formalism [50]. C_i are the liquid drop model stiffness parameters of the fragments. Here we only enable quadrupole deformation ($\lambda = 2$). σ is the coefficient of surface tension which follows $4\pi R_i^2\sigma = a_s A_i^{2/3}$, and the nuclear radius is R_i. $B(Z_i,N_i)$ ($i = 1, 2$) and $B(Z,N)$ are the negative binding energies of the fragment (Z_i,N_i) and the composite system (Z,N), respectively. Here we adopt binding energy data from Ref. [52], in which calculations are based on the finite-range droplet macroscopic and the folded-Yukawa single-particle microscopic nuclear-structure models.

In the collision process, the evolutions of quadrupole deformations of projectile-like fragments (PLFs) and target-like fragments (TLFs) proceed from the initial configuration as

$$\beta'_{\rm T}(t) = \beta_{\rm T}\exp(-t/\tau_\beta) + \beta_1[1-\exp(-t/\tau_\beta)],$$
$$\beta'_{\rm P}(t) = \beta_{\rm P}\exp(-t/\tau_\beta) + \beta_2[1-\exp(-t/\tau_\beta)], \quad (8)$$

where the deformation relaxation is $\tau_\beta = 4\times10^{-21}$ s. β_1, β_2 are the ground-state quadrupole deformations of TLFs and PLFs. The ground-state quadrupole deformation of projectile (target) is $\beta_{\rm P}$ ($\beta_{\rm T}$). $\beta'_{\rm T}(t)$ and $\beta'_{\rm P}(t)$ are the quadrupole deformations of TLFs and PLFs at moment t.

The cross sections of the surviving fragments produced in MNT reactions and the fusion-evaporation residue cross sections are evaluated by

$$\sigma_{\rm sur}(Z_1,N_1,E_{\rm c.m.}) = \frac{\pi\hbar^2}{2\mu E_{\rm c.m.}}\sum_{J=0}^{J_{\rm max}}(2J+1) \times\int f(B)T(E_{\rm c.m.},J,B)\sum_s P(Z'_1,N'_1,E'_1,J'_1,B) \times W_{\rm sur}(Z'_1,N'_1,E'_1,J'_1,s)dB \quad (9)$$

and

$$\sigma^s_{\rm ER}(E_{\rm c.m.}) = \frac{\pi\hbar^2}{2\mu E_{\rm c.m.}}\sum_{J=0}^{J_{max}}(2J+1)T(E_{\rm c.m.},J) \times P_{\rm CN}(E_{\rm c.m.},J)W^s_{\rm sur}(E_{\rm c.m.},J), \quad (10)$$

respectively. μ is the reduced mass of relative motion. The transmission probability $T(E_{\rm c.m.},J)$ is calculated by the Hill-Wheeler formula in combination with the barrier distribution function. E_1 and J_1 are the excitation energy and the angular momentum for the fragment (Z_1,N_1). The maximal angular momentum $J_{\rm max}$ is taken to be the grazing collision of two nuclei. The survival probability $W_{\rm sur}$ of each fragment is evaluated with a statistical approach based on the Weisskopf evaporation theory [53], in which the excited primary fragments are cooled in evaporation channels $s(Z_s,N_s)$ by γ rays, light particles (neutrons, protons, α, etc.) in competition with the binary fission via $Z_1 = Z'_1 - Z_s$ and $N_1 = N'_1 - N_s$:

$$P_{\rm CN}(E_{\rm c.m.},J) = \sum_{Z_1=1}^{Z_{\rm BG}}\sum_{N_1=1}^{N_{\rm BG}}P(Z_1,N_1,\tau_{\rm int},J). \quad (11)$$

$P_{\rm CN}(E_{\rm c.m.},J)$ is the fusion probability which sums over all the fragments probability located outside of the BG (Businaro-Gallone) point. The transfer cross section is smoothed with the barrier distribution. The total kinetic energy (TKE) of the primary fragment is evaluated by

$$\mathrm{TKE}(A_1) = E_{\rm c.m.} + Q_{\rm gg} - E^{\rm diss}(A_1), \quad (12)$$

where $Q_{\rm gg} = M_{\rm P} + M_{\rm T} - M_{\rm PLF} - M_{\rm TLF}$ and $E_{\rm c.m.}$ is the incident energy in the center-of-mass frame. The masses $M_{\rm P}$, $M_{\rm T}$, $M_{\rm PLF}$, and $M_{\rm TLF}$ correspond to projectile, target, PLF and TLF, respectively. Here we apply the nuclear ground-state masses data from literature [52].

III. RESULTS AND DISCUSSION

In heavy-ion collisions that overcome the Coulomb barrier, kinetic energy of relative motion transforms rapidly into internal excitation of the dinuclear system at the contact point. The interaction potential distribution vs distance, interaction time vs impact parameter, and internal excitation energy vs reaction time for the system of ^{48}Ca + ^{248}Cm reactions at incident energy $E_{\rm lab} = 5.5$ MeV/nucleon are shown in Fig. 1. The interaction potential is calculated as a function of the surface distance between two heavy partners. From panel (a), one can see that the Coulomb barrier of the colliding system is about 185 MeV and the quasifission barrier is several MeV. The potential pocket is located almost near the contact point. The reaction time is calculated by deflection function, plotted as a function of angular momentum, which decreases exponentially with increasing angular momentum. The internal excitation energy dissipating in the dinuclear system increases exponentially with increasing evolution time. The existence of the pocket in the entrance channel is crucial for the compound nucleus formation in fusion reactions, which is the input physical quantity in calculating capture cross section. The barrier is taken as the potential value at the touching configuration and the nucleus-nucleus potential is calculated with the same

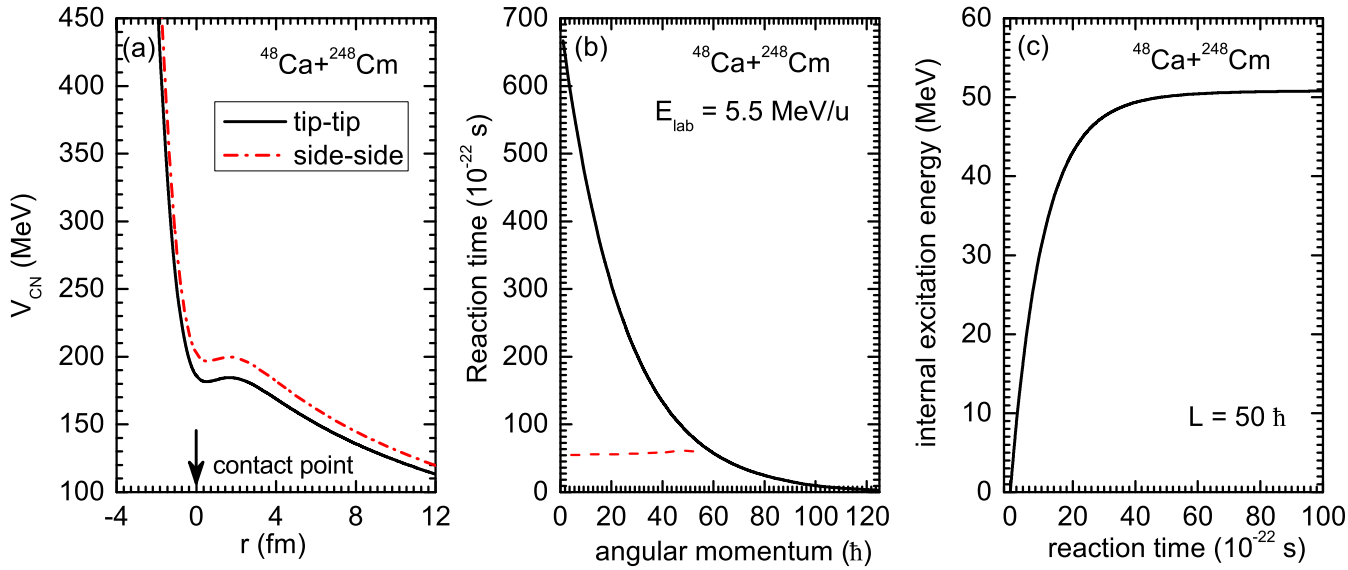

FIG. 1. Solid black line and red dash-dots line are interaction potential of the tip-tip and side-side collisions as a function of surface distance in the reaction of $^{48}\mathrm{Ca} + {}^{248}\mathrm{Cm}$ in panel (a); In panel (b), Solid black and red dash lines corresponding to the reaction the "boundary" of timescale between complete fusion and MNT reactions; The internal excitation energy of $^{48}\mathrm{Ca} + {}^{248}\mathrm{Cm}$ collision at $E_{\mathrm{lab}} = 5.5$ MeV/nucleon with impact parameter $L = 50\ \hbar$ in panel (c).

approach in fusion reactions [54]. According to Fig. 1, it was found that there are few MeV potential pockets for heavy systems, because of the strong Coulomb repulsion between two colliding partners with $Z_1Z_2 = 1860$. Lighter collision systems have a deeper potential pocket, relatively. A deeper potential pocket collision system leads to a correspondingly longer reaction time. With impact parameter $L = 50\hbar$ for the $^{48}\mathrm{Ca} + {}^{248}\mathrm{Cm}$ reaction, the timescale of reaching almost the equilibrium state for incident energy dissipating in internal excitation energy is about 5.7×10^{-21}s.

Nucleons can be transferred between the collision partners resulting in the internal degree of freedom characterizing the nuclear states encountering a rapid rearrangement along the potential energy surface (PES) as well as dissipating their kinetic energy and angular momentum. The calculation of a multidimensional adiabatic PES for a heavy nuclear system is a quite complicated physical problem, and is still an open problem. In this work, the PES for tip-tip collisions of $^{48}\mathrm{Ca} + {}^{248}\mathrm{Cm}$ is calculated by Eq. (6) as a diabatic type with frozen distance, shown in Fig. 2(b). The solid black line, solid black circle, and solid red triangle are valley value, projectile-target position, and compound nuclei, respectively. The valley value in PES is listed as a function of mass, shown in Fig. 2(a). The inner fusion barrier of the collision partners is $B_{\mathrm{fus}} = 5.24$ MeV, which means that it needs to overcome 5.24 MeV barrier energy to fuse. The DNS fragments towards the mass symmetric valley release positive energy, which is available for nucleon transfer. The spectra exhibit a symmetric distribution for each isotopic chain. The valley in the PES is close to the β-stability line and enables the diffusion of the fragment probability. Figure 3 shows the calculation correlation of the total kinetic energy (TKE)

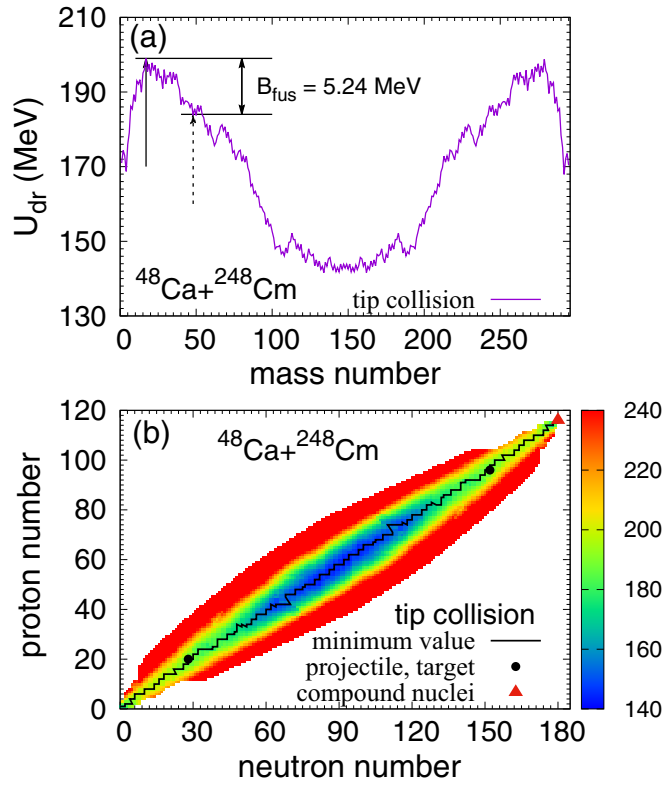

FIG. 2. The driver potentials of $^{48}\mathrm{Ca} + {}^{248}\mathrm{Cm}$ at tip-tip collision. Potential energy surface as a function of mass calculated at two fixed distances between projectile and target. The arrows and black solid circles indicate the entrance channel. The solid triangle is the compound nucleus. The two solid lines are minimum values in two-dimensional potential energy surfaces.

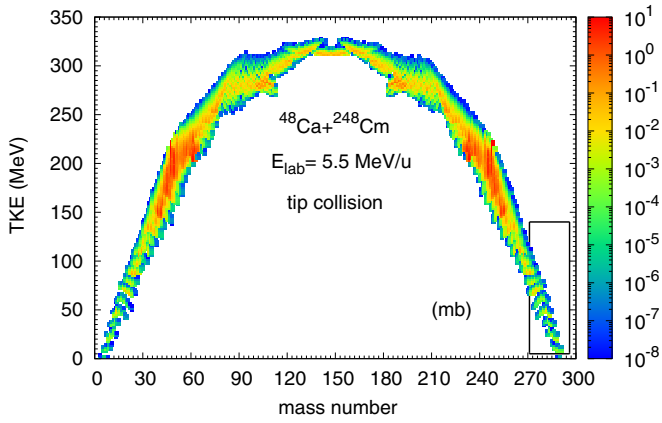

FIG. 3. Calculated TKE-mass distribution of primary reaction products in the collision of $^{48}\mathrm{Ca} + ^{248}\mathrm{Cm}$ at $E_{\mathrm{lab}} = 5.5$ MeV/nucleon. The fragments in square areas overcome the inner fusion barrier (Businaro-Gallone point).

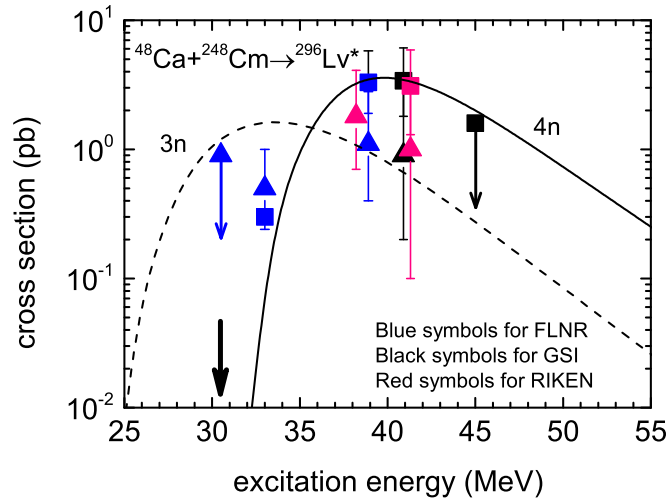

FIG. 4. The calculated evaporation residues as a function of excitation energy in the reaction $^{48}\mathrm{Ca}(^{248}\mathrm{Cm}, xn)$. Cross sections and cross-section limits of the reaction $^{48}\mathrm{Ca} + ^{248}\mathrm{Cm} \rightarrow {}^{296}116^{*}$ measured at GSI [41], FLNR [40], and RIKEN [42]. The data for synthesis of $^{293}116$ ($3n$ channel, triangles) and $^{292}116$ ($4n$ channel, squares) are shown.

and mass distributions of the reaction products along with inclusion mass distribution for the $^{48}\mathrm{Ca} + ^{248}\mathrm{Cm}$ reaction at a near-barrier energy of $E_{\mathrm{lab}} = 5.5$ MeV/nucleon. These calculations agree roughly well with experimental data [55]. They are consistent with calculations by Langevin-type dynamical equations [56]. In most of the damped collisions the interaction time is rather short (several units of 10^{-21} s). These fast events correspond to grazing collisions with intermediate impact parameters, which are shown by the areas around projectile-target points. A large amount of kinetic energy is dissipated here very fast at relatively low mass transfer (more than 45 MeV during several units of 10^{-21} s). The other events correspond to much slower collisions with a large overlap of nuclear surface and significant rearrangement of nucleons. In the TKE-mass plot, these events spread over a wide region of mass fragments. These fragments in the square areas indicate overcoming the inner barrier (Businaro-Gallone point), which means they can lead to compound nuclei, in the framework of the DNS model. Predicted and experimental excitation functions of $3n$ and $4n$ channels for production of livermorium ($Z = 116$) in the ^{48}Ca induced reactions are shown in Fig. 4. The experimental data have been obtained at FLNR, GSI, and RIKEN, shown as blue, black, and red symbols, respectively. Early or late, FLNR [40], GSI [41], and RIKEN [42] obtained excitation functions of $3n$ and $4n$ evaporation channels for production of superheavy element with $Z = 116$ in collisions of $^{48}\mathrm{Ca} + ^{248}\mathrm{Cm}$, respectively.

At FLNR, at lower beam energies three irradiations were performed in Dubna in June–July and November–December 2000 and in January and April–May 2001 [40]. At $E^* = 30.5$ MeV a cross-section limit of 0.9 pb was reached. At $E^* = 33.0$ MeV, three decay chains were measured resulting in a cross section of $(0.5^{+0.5}_{-0.26})$ pb, and were assigned to $^{293}116$. At the same excitation energy, a cross-section limit of 0.3 pb was obtained for the $4n$ channel. The highest energy studied resulted in $E^* = 38.9$ MeV. At this energy, six decay chains were measured and assigned to $^{292}116$ resulting in a cross section of $(3.3^{+2.5}_{-1.4})$ pb for the $4n$ channel. Also at the same energy two chains from the $3n$ channel were measured resulting in a cross section of $(1.1^{+1.7}_{-0.7})$ pb. This experiment was performed in April–May, 2004 [57]. Four cross-section data marked by solid blue symbols are shown in Fig. 4.

At GSI, at an energy $E^* = 40.9$ MeV, they detected six decay chains; four events were assigned to the $4n$ channel resulting in a cross section of $(3.4^{+2.7}_{-1.6})$ pb, and one from the

TABLE I. Calculated and measured cross sections (in μb) of isotopes are collected for the reaction $^{48}\mathrm{Ca} + ^{248}\mathrm{Cm}$ near Coulomb barrier energies. The errors are listed in parentheses after the cross-section values.

Isotope	Expt. 270 MeV Ref. [47]	Expt. 247–263 MeV Ref. [44]	Expt. 272–288 MeV Ref. [44]	Calc. 264 MeV This work
^{245}Bk		40 (40%)	67 (20%)	35.0
^{246}Bk		360 (10%)	480 (15%)	69.6
^{248}Bk		2900 (6%)	2680 (15%)	224.0
^{250}Bk		2520 (5%)	2920 (10%)	1061.0
^{246}Cf		1.8 (2%)	1 (20%)	2.8
^{248}Cf		260 (2%)	210 (6%)	151.0
^{250}Cf		2380 (7%)	1935 (2%)	930.0
^{252}Cf	<58.0	225 (4%)	220 (15%)	81.0
^{253}Cf		12 (20%)	4 (15%)	2.9
^{254}Cf	>0.12	1.5 (30%)	1 (25%)	0.5
^{250}Es		6.6 (40%)		5.5
^{252}Es		30 (15%)	24 (5%)	12.0
^{253}Es		10 (10%)	7.8 (15%)	26.0
^{254}Es	0.9 (10%)	2 (15%)	1.4 (15%)	1.5
^{252}Fm		0.11 (35%)	0.06 (20%)	0.8
^{254}Fm	0.9 (10%)	0.81 (5%)	0.7 (8%)	1.1
^{255}Fm		0.9 (30%)	0.62 (10%)	0.47
^{256}Fm	39 nb (36%)	0.24 (20%)	0.14 (15%)	0.07

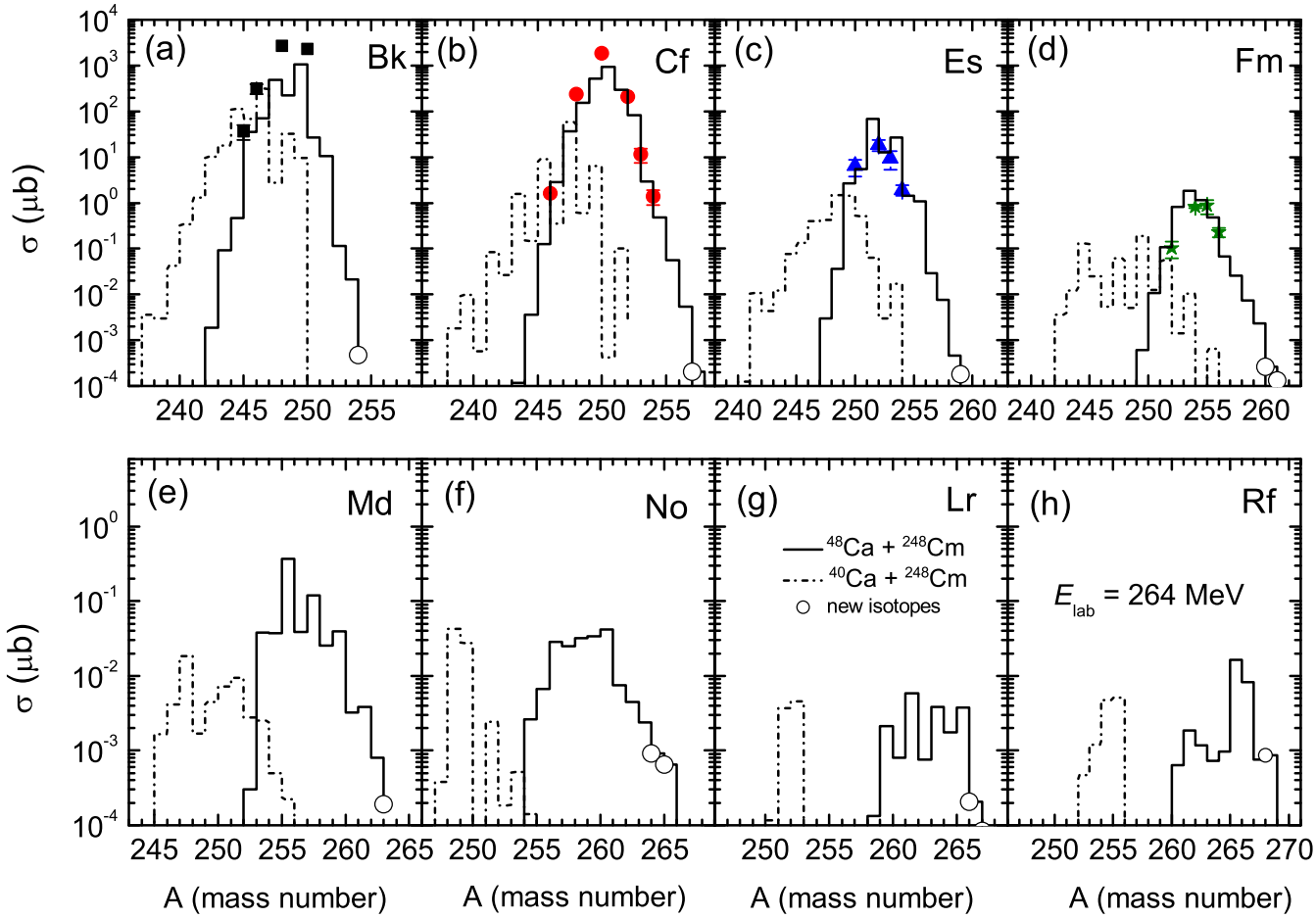

FIG. 5. Predicted and measured isotopic distributions for the production of target-like fragments with $Z = 97$–100 in the collisions of ^{48}Ca + ^{248}Cm. The experimental data are taken from Gesellschaft für Schwerionenforschung (GSI, Germany) [44] and Lawrence Berkeley Laboratory (LBL, USA) [45].

other two events was assigned to the $3n$ channel. Therefore the cross section of $(0.9^{+2.1}_{-0.7})$ pb is presented here, which is valid for the event definitely assigned to ^{293}116. No event was observed in the second part of the experiment at $E^* = 45.0$ MeV, resulting in a one-event cross-section limit of 1.6 pb. Three cross-section data marked by solid black symbols are shown in Fig. 4.

At RIKEN, the fusion reaction ^{48}Ca + ^{248}Cm $\rightarrow$ ^{296}Lv* was investigated using the gas-filled recoil ion separator GARIS. The reaction was studied at excitation energies of 41.3 and 38.2 MeV. A total of seven decay chains were observed. Three of the chains were assigned to the decay of ^{292}Lv and three to the decay of ^{293}Lv. The resulting cross sections are $\sigma_{4n} = (3.1^{+2.8}_{-1.8})$ pb at $E^* = 41.3$ MeV and $\sigma_{3n} = (1.0^{+2.4}_{-0.9})$ pb and $\sigma_{3n} = (1.8^{+2.3}_{-1.1})$ pb at $E^* = 41.3$ and 38.2 MeV, respectively. In the case of unobserved decay chains, the one-event cross-section limits are 1.9 and 1.6 pb at $E^* =$ 41.3 and 38.2 MeV, respectively. Three cross-section data are marked by solid red symbols in Fig. 4. In theoretical calculation, Q_{value} of the reactions ^{48}Ca + ^{248}Cm $\rightarrow$ ^{296}Lv* is -166.57 MeV and the V_{Bass} potential is 197.12 MeV, which is indicated by a solid black arrow. The dashed line and solid line are calculated excitation functions corresponding to $3n$ and $4n$ evaporation channels. One can see from Fig. 4 that calculated excitation functions have a good agreement with all the available experimental data [40–42].

In the collision of ^{48}Ca + ^{248}Cm at energies near the Coulomb barrier, the MNT products are dominant in all isotopic yields. In the 1980s, to study the role of neutron-rich projectile ^{48}Ca in enhancing the yields of neutron-rich actinides and to determine what effect the eight fewer neutrons in ^{48}Ca have on the mass distribution, two series of experiments were performed at LBL and at GSI using radiochemical methods and online gas-jet transport of short-lived reaction products combined with electronic detection systems [44]. Above-target isotopes from Bk to Fm and below-target isotopes of Rn, Ra, Ac, Th, U, and Pu were observed in the reactions of ^{48}Ca + ^{248}Cm at incident energies $E_{lab} =$ 223–239, 248–263, 247–263, 272–288, and 304–318 MeV. The maximum yields of above-target isotopes were around $E_{lab} = 248$–263 MeV. In this paper, we report on production of Bk, Cf, Es, and Fm only. The production of below-target isotopes has been discussed in paper [58].

In the year 2000, experiments of ^{48}Ca + ^{248}Cm at incident energies $E_{lab} = 265.4$, 270.2 MeV were performed at GSI [47]. In the experiment, fusion products and target-like

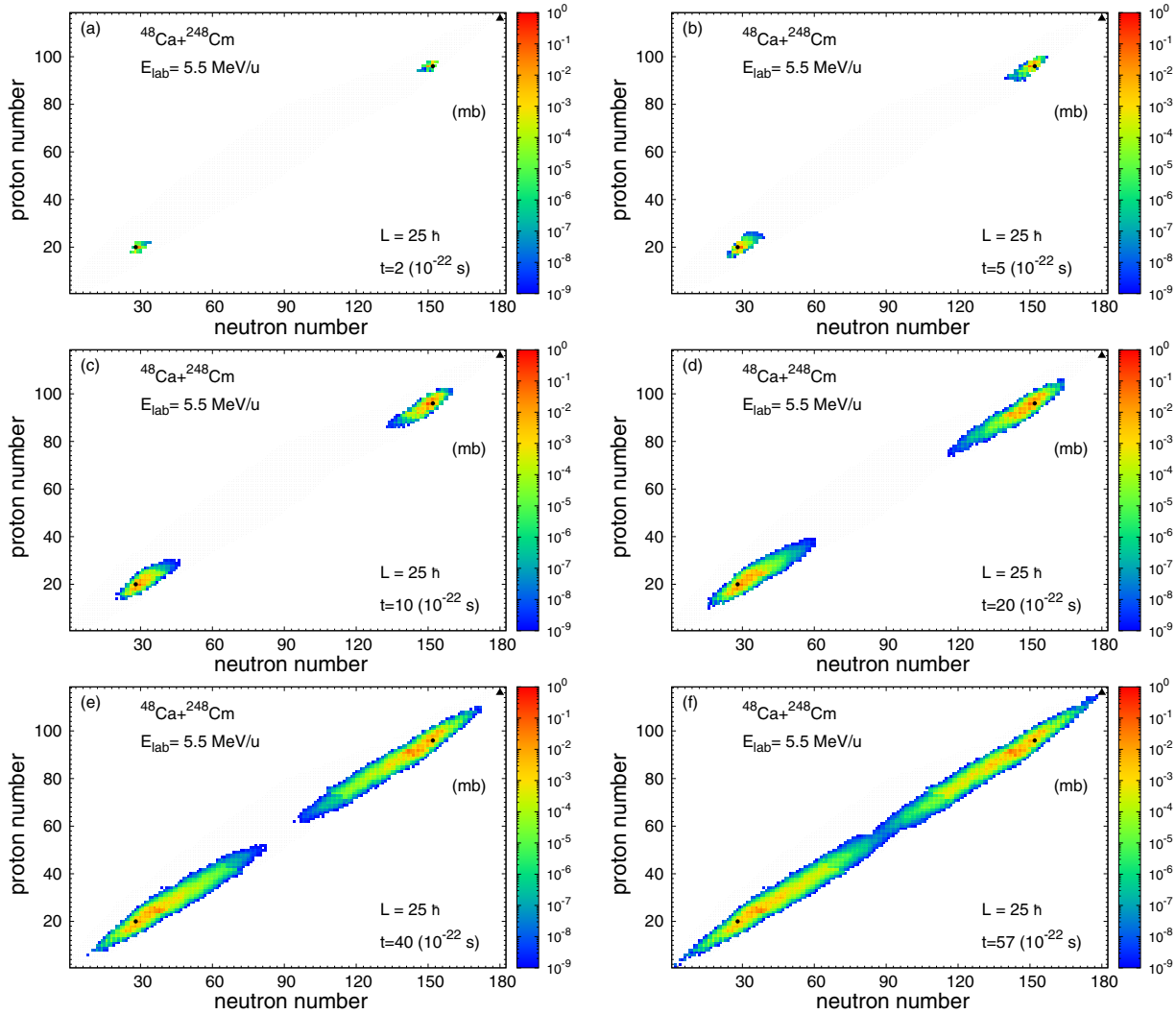

FIG. 6. The production cross sections of primary fragments in collisions of ^{48}Ca on ^{248}Cm at the incident energy of 5.5 MeV/nucleon with the initial angular momentum of $L = 25\hbar$. Isotope yields in panels (a)–(f) correspond to evolution times 2×10^{-22} s, 4×10^{-22} s, 1×10^{-21} s, 2×10^{-21} s, 4×10^{-21} s, and 5.7×10^{-21} s, respectively.

transfer reaction products were measured using the SHIP detector. Due to short dection time (two days) and limited seperation method, several above target isotopes have been obtained. They are ^{252,254}Cf, ^{254,256}Es, ^{254,256}Fm listed in Table I.

The cross sections measured in Ref. [46] for the same isotopes and same collision system are also listed for comparison. The results from both experiments are in quite good agreement despite the different experimental techniques and systematic uncertainties. For example, cross sections for the directly populated nuclides ^{254}Cf and ^{254}Es are in agreement within factors of $\approx$1.8 and 1.5 compared to the cross sections presented in paper [46]. For the same reaction system, different separation methods can result in discrepancies of several orders of magnitude. Predicted and identified MNT products from Bk to Fm along with the measured cross sections are presented in Fig. 5. Compared to the measured cross section, calculations have a reasonably good agreement. Calculation and experimental data reveal a trend that the cross section of certain MNT products decreases on average by one order of magnitude with the transfer of each proton from the projectile to the target nucleus, because of the heavier above-target isotopes and the smaller fission barriers. Here predictions have been made for unknown isotopes ^{254}Bk, ^{257}Cf, ^{259}Es, ^{260}Fm, ^{263}Md, ^{264,265}No, ^{266}Lr, and ^{268}Rf, which are 0.4, 0.2, 0.1, 0.2, 0.2, 0.9, 0.6, 0.2, and 1 nb respectively. Collisions of atomic nuclei are ideal to investigate equilibration and dissipative process in quantum many-body systems [59,60]. Exploring nuclear dynamics in complete and incomplete fusion for heavy-ion collisions can be used to understand the interplay between equilibrium and dissipation in a quantum system. In the collision process, nucleons can diffuse from target to compound nuclei, where probabilities of all formed fragments will be exported at every moment. Then, the dynamical process of isotopic yields from preequilibrium to equilibrium can reveal a boundary line between complete fusion and multinucleon transfer reactions. The timescale for mass equilibrium ($\approx 10^{-20}$ s) is found to

be larger than the timescale for kinetic energy dissipations, which is on the order of 10^{-21} s. In our approach, collisions of ^{48}Ca + ^{248}Cm at $E_{\rm lab} = 5.5$ MeV/nucleon with impact parameter $L = 25\hbar$, dynamical nucleon transfer between projectile and target is exhibited by plotting graphs for all fragments' productions in different timescales, 2×10^{-22} s, 4×10^{-22} s, 1×10^{-21} s, 2×10^{-21} s, 4×10^{-21} s, and 5.7×10^{-21} s, shown in Figs. 6(a)–6(f), respectively. One can see that the composite system starts to fuse compound nuclei from 5.7×10^{-21} s. We consider the timescale as a boundary between complete and incomplete fusion. The moments of collision partners fusing to compound nuclei are found in the diffusion process. We calculate and find all these moments corresponding to all impact parameters. We plotted all these moments as a red dashed line shown in Fig. 1(b). It was found that the upper limit of impact parameter for the synthesis of a superheavy element $Z = 116$ is $L = 56\hbar$, mainly because the dissipating energy of colliding system almost reached equilibrium. The boundary line between CF and MNT has been found to be around 5.7×10^{-21} s. It is worth mentioning that our calculations for equilibrium timescales of fragment mass asymmetry and kinetic dissipation are consistent with calculations from time-dependent Hartree-Fock (TDHF) and time-dependent random-pahse approximation (TDRPA) approaches [61].

IV. CONCLUSIONS

In summary, production of above-target isotopes and compound nuclei has been investigated within the DNS model through complete fusion-evaporation and multinucleon transfer reactions, for the MNT products of Bk, Cf, Es, Fm and for the fusion-evaporation products of ^{292,293}Lv. In the collision process, kinetic energy dissipates in internal excitation energy to heat up the composite system. The nucleon transfer takes place at the touching configuration of two colliding nuclei under the PES. The valley shape of the PES influences the formation of primary fragments and leads to the production of quasifission isotopes. The PES enabled here is a diabatic type, which is derived by $Q_{\rm gg}$ value, double-folding nuclear potential, and Coulomb potential. The TKE-mass distribution of multinucleon transfer products reveals some quantities, namely, reaction mechanisms, dissipating energy, and shell and structure effects. The calculation can reasonably explain both experimental results of complete fusion-evaporation products and multinucleon transfer fragments for ^{48}Ca + ^{248}Cm. The available experiment data are obtained from laboratories all over the world. In our calculation, the diffusion pathway from the target to compound nuclei has been indicated, derived by dynamic competition with deep-inelastic reactions and quasifission for two heavy systems. The excitation functions of producing superheavy isotopes ^{292,293}Lv are composed of experimental data from three different laboratories, GSI, FLNR, and RIKEN.

We compare their experimental data obtained from two groups, for target-like fragments in the collision of ^{48}Ca + ^{248}Cm: those from GSI and LBL in the years 1986 and 2010, respectively. It is found that the obtained isotopic cross section is highly dependent on the identification method. In particular, for below-target isotopes ($Z < 96$), the cross section obtained by radiochemical method is three orders of magnitude larger than that obtained by decay spectroscopy. However, the cross section of above-target nuclei ($Z > 96$) from both experiments are quite consistent despite the different experimental techniques and systematic uncertainties. The effective impact parameter of these two colliding partners leading to compound nuclei is from central collison to $L = 52\hbar$. The timescale between complete and incomplete reactions is about 5.7×10^{-21} s with effective impact parameters. We predict that synthesis cross sections of unknown rare isotopes ^{254}Bk, ^{257}Cf, ^{259}Es, ^{260}Fm, ^{263}Md, ^{264,265}No, ^{266}Lr, and ^{268}Rf are around nanobarn scale in collisions of ^{48}Ca + ^{248}Cm near Coulomb barrier energies.

ACKNOWLEDGMENTS

This work is supported by the National Science Foundation of China (NSFC) (Grants No. 12105241 and No. 12175072), NSF of Jiangsu Province (Grants No. BK20210788), the Jiangsu Provincial Double-Innovation Doctor Program (Grant No. JSSCBS20211013), the University Science Research Project of Jiangsu Province (Grants No. 21KJB140026), and Lv Yang Jin Feng of Yangzhou City (Grant No. YZLYJFJH2021YXBS130). This project is funded by the Key Laboratory of High Precision Nuclear Spectroscopy, Institute of Modern Physics, Chinese Academy of Sciences (CAS). This work is supported by the Strategic Priority Research Program of CAS (Grant No. XDB34010300).

[1] Y. T. Oganessian and V. K. Utyonkov, Superheavy nuclei from ^{48}Ca-induced reactions, Nucl. Phys. A **944**, 62 (2015).

[2] V. K. Utyonkov, N. T. Brewer, and Yu. Ts. Oganessian, K. P. Rykaczewski, F. S. Abdullin, S. N. Dmitriev *et al.*, Experiments on the synthesis of superheavy nuclei ^{284}Fl and ^{285}Fl in the ^{239,240}Pu + ^{48}Ca reactions, Phys. Rev. C **92**, 034609 (2015).

[3] S. Hofmann, Radiochim, Synthesis of superheavy elements by cold fusion, Acta. **99**, 405 (2011).

[4] C. E. Düllmann, R. D. Herzberg, W. Nazarewicz *et al.*, Special issue on superheavy elements - Foreword, Nucl. Phys. A **944**, 1 (2015).

[5] K. Morita, SHE research at RIKEN/GARIS, Nucl. Phys. A **944**, 30 (2015).

[6] L. Stavsetra, K. E. Gregorich, J. Dvorak, P. A. Ellison, I. Dragojevic, M. A. Garcia, and H. Nitsche, Independent Verification of Element 114 Production in the ^{48}Ca + ^{242}Pu Reaction, Phys. Rev. Lett. **103**, 132502 (2009).

[7] Z. G. Gan, Z. Qin, H. M. Fan *et al.*, A new alpha-particle-emitting isotope ^{259}Db, Eur. Phys. J. A **10**, 21 (2001).

[8] Z. G. Gan, J. S. Guo, X. L. Wu *et al.*, New isotope ^{265}Bh, Eur. Phys. J. A **20**, 385 (2004).

[9] Z. Y. Zhang, Z. G. Gan, L. Ma *et al.*, Observation of the superheavy nuclide ^{271}Ds, Chin. Phys. Lett. **29**, 012502 (2012).

[10] A. G. Artukh, V. V. Avdeichikov, G. F. Gridnev, V. L. Mikheev, V. V. Volkov, and J. Wilczynski, New isotopes ^{29,30}Mg, ^{31,32,33}Al, ^{33,34,35,36}Si, ^{35,36,37,38}P, ^{39,40}S, and ^{41,42}Cl produced in bombardment of a ^{232}Th target with 290 MeV ^{40}Ar ions, Nucl. Phys. A **176**, 284 (1971).

[11] A. G. Artukh, G. F. Gridnev, V. L. Mikheev, V. V. Volkov, and J. Wilczynski, Multinucleon transfer reactions in the ^{232}Th + ^{22}Ne system, Nucl. Phys. A **211**, 299 (1973).

[12] A. G. Artukh, G. F. Gridnev, V. L. Mikheev, V. V. Volkov, and J. Wilczynski, Transfer reactions in the interaction of ^{40}Ar with ^{232}Th, Nucl. Phys. A **215**, 91 (1973).

[13] K. D. Hildenbrand, H. Freiesleben, F. Phlhofer, W. F. W. Schneider, R. Bock, D. V. Harrach, and H. J. Specht, Reaction between ^{238}U and ^{238}U at 7.42 MeV/Nucleon, Phys. Rev. Lett. **39**, 1065 (1977).

[14] P. Glässel, D. V. Harrach, Y. Civelekoglu, R. Männer, H. J. Specht, J. B. Wilhelmy *et al.*, Three-Particle Exclusive Measurements of the Reactions ^{238}U + ^{238}U and ^{238}U + ^{248}Cm, Phys. Rev. Lett. **43**, 1483 (1979).

[15] K. J. Moody, D. Lee, R. B. Welch, K. E. Gregorich, G. T. Seaborg, R. W. Lougheed, and E. K. Hulet, Actinide production in reactions of heavy ions with ^{248}Cm, Phys. Rev. C **33**, 1315 (1986).

[16] R. B. Welch, K. J. Moody, K. E. Gregorich, D. Lee, and G. T. Seaborg, Dependence of actinide production on the mass number of the projectile: Xe+ ^{248}Cm, Phys. Rev. C **35**, 204 (1987).

[17] E. M. Kozulin, E. Vardaci, G. N. Knyazheva, A. A. Bogachev, S. N. Dmitriev, I. M. Itkis *et al.*, Mass distributions of the system ^{136}Xe + ^{208}Pb at laboratory energies around the Coulomb barrier: A candidate reaction for the production of neutron-rich nuclei at $N = 126$, Phys. Rev. C **86**, 044611 (2012).

[18] J. S. Barrett, W. Loveland, R. Yanez *et al.*, ^{136}Xe + ^{208}Pb reaction: A test of models of multinucleon transfer reactions, Phys. Rev. C **91**, 064615 (2015).

[19] Y. X. Watanabe, Y. H. Kim, S. C. Jeong, Y. Hirayama, N. Imai, H. Ishiyama *et al.*, Pathway for the Production of Neutron-Rich Isotopes around the $N = 126$ Shell Closure, Phys. Rev. Lett. **115**, 172503 (2015).

[20] E. M. Kozulin, V. I. Zagrebaev, G. N. Knyazheva, I. M. Itkis, K. V. Novikov, M. G. Itkis *et al.*, Inverse quasifission in the reactions ^{156,160}Gd + ^{186}W, Phys. Rev. C **96**, 064621 (2017).

[21] S. Wuenschel, K. Hagel, M. Barbui, J. Gauthier, X. G. Cao, R. Wada *et al.*, Experimental survey of the production of α-decaying heavy elements in ^{238}U + ^{232}Th reactions at 7.5–6.1 MeV/nucleon, Phys. Rev. C **97**, 064602 (2018).

[22] V. Zagrebaev and W. Greiner, Low-energy collisions of heavy nuclei: Dynamics of sticking, mass transfer and fusion, J. Phys. G **34**, 1 (2007); New way for the production of heavy neutron-rich nuclei, **35**, 125103 (2008).

[23] V. Zagrebaev and W. Greiner, Synthesis of superheavy nuclei: A search for new production reactions, Phys. Rev. C **78**, 034610 (2008); Production of New Heavy Isotopes in Low-Energy Multinucleon Transfer Reactions, Phys. Rev. Lett. **101**, 122701 (2008).

[24] C. Golabek and C. Simenel, Collision Dynamics of Two ^{238}U Atomic Nuclei, Phys. Rev. Lett. **103**, 042701 (2009).

[25] K. Sekizawa and K. Yabana, Time-dependent Hartree-Fock calculations for multinucleon transfer and quasifission processes in the ^{64}Ni + ^{238}U reaction, Phys. Rev. C **93**, 054616 (2016).

[26] L. Guo, C. Simenel, L. Shi, and C. Yu, The role of tensor force in heavy-ion fusion dynamics, Phys. Lett. B **782**, 401 (2018).

[27] X. Jiang and N. Wang, Production mechanism of neutron-rich nuclei around N = 126 in the multi-nucleon transfer reaction ^{132}Sn + ^{208}Pb, Chin. Phys. C **42**, 104105 (2018).

[28] A. Winther, Grazing reactions in collisions between heavy nuclei, Nucl. Phys. A **572**, 191 (1994); Dissipation, polarization and fluctuation in grazing heavy-ion collisions and the boundary to the chaotic regime, **594**, 203 (1995).

[29] http://www.to.infn.it/nanni/grazing.

[30] K. Zhao, Z. Li, N. Wang, Y. Zhang, Q. Li, Y. Wang, and X. Wu, Production mechanism of neutron-rich transuranium nuclei in ^{238}U + ^{238}U, Phys. Rev. C **92**, 024613 (2015).

[31] C. Li, F. Zhang, J. J. Li, L. Zhu, J. L. Tian, N. Wang, and F. S. Zhang, Multinucleon transfer in the ^{136}Xe + ^{208}Pb reaction, Phys. Rev. C **93**, 014618 (2016).

[32] C. W. Shen, D. Boilley, Q. F. Li, J. J. Shen, and Y. Abe, Fusion hindrance in reactions with very heavy ions: Border between normal and hindered fusion, Phys. Rev. C **83**, 054620 (2011).

[33] D. Boilley, H. L. Lü, C. W. Shen, Y. Abe, and B. G. Giraud, Fusion hindrance of heavy ions: Role of the neck, Phys. Rev. C **84**, 054608 (2011).

[34] Z. Q. Feng, G. M. Jin, and J. Q. Li, Production of heavy isotopes in transfer reactions by collisions of ^{238}U + ^{238}U, Phys. Rev. C **80**, 067601 (2009).

[35] G. G. Adamian, N. V. Antonenko, V. V. Sargsyan, and W. Scheid, Possibility of production of neutron-rich Zn and Ge isotopes in multinucleon transfer reactions at low energies, Phys. Rev. C **81**, 024604 (2010); Predicted yields of new neutron-rich isotopes of nuclei with $Z = 64$–80 in the multinucleon transfer reaction ^{48}Ca + ^{238}U, **81**, 057602 (2010).

[36] P. H. Chen, F. Niu, W. Zuo, and Z. Q. Feng, Approaching the neutron-rich heavy and superheavy nuclei by multinucleon transfer reactions with radioactive isotopes, Phys. Rev. C **101**, 024610 (2020).

[37] X. J. Bao, S. Q. Guo, H. F. Zhang, and J. Q. Li, Dynamics of complete and incomplete fusion in heavy-ion collisions, Phys. Rev. C **97**, 024617 (2018).

[38] X. J. Bao, Possibilities for synthesis of new transfermium isotopes in multinucleon transfer reactions, Phys. Rev. C **104**, 034604 (2021).

[39] L. Zhu, Shell inhibition on production of $N = 126$ isotones in multinucleon transfer reactions, Phys. Lett. B **816**, 136226 (2021).

[40] Yu. Ts. Oganessian, V. K. Utyonkov, and Yu. V. Lobanov, Observation of the decay of ^{292}116, Phys. Rev. C **63**, 011301(R) (2000).

[41] S. Hofmann, S. Heinz, R. Mann *et al.*, The reaction ^{48}Ca + ^{248}Cm → ^{296}116* studied at the GSI-SHIP, Eur. Phys. J. A **48**, 62 (2012).

[42] D. Kaji, K. Morita1, K. Morimoto *et al.*, Study of the Reaction ^{48}Ca + ^{248}Cm → ^{296}116* at RIKEN-GARIS, J. Phys. Soc. Jpn. **86**, 034201 (2017).

[43] H. M. Devaraja, S. Heinz, O. Beliuskina, V. Comas, S. Hofmann, C. Hornung *et al.*, Observation of new neutron-deficient isotopes with $Z \geqslant 92$ in multinucleon transfer reactions, Phys. Lett. B **748**, 199 (2015).

[44] D. C. Hoffman, M. M. Fowler, and W. R. Daniels, H. R. vonGunten, D. Lee, K. J. Moody *et al.*, Excitation functions for production of heavy actinides from interactions of ^{40}Ca and ^{48}Ca ions with ^{248}Cm, Phys. Rev. C **31**, 1763 (1985).

[45] H. Giggeler, W. Bruchle, M. Brugger, M. Schadel, K. Summerer, G. Wirth *et al.*, Production of cold target-like

fragments in the reaction of ^{48}Ca + ^{248}Cm, Phys. Rev. C **33**, 1983 (1986).

[46] S. Heinz, H. M. Devaraja, O. Beliuskina *et al.*, Synthesis of new transuranium isotopes in multinucleon transfer reactions using a velocity filter, Eur. Phys. J. A **52**, 278 (2016).

[47] H. M. Devaraja, S. Heinz, O. Beliuskina *et al.*, Population of nuclides with $Z \leqslant 98$ in multi-nucleon transfer reactions of ^{48}Ca + ^{248}Cm, Eur. Phys. J. A **55**, 25 (2019).

[48] G. Wolschin and W. Nörenberg, Analysis of relaxation phenomena in heavy-ion collisions, Z. Phys. A **284**, 209 (1978).

[49] Z. Q. Feng, G. M. Jin, F. Fu, and J. Q. Li, Isotopic dependence of production cross-sections of superheavy nuclei in hot fusion reactions, Chin. Phys. C **31**, 366 (2007).

[50] P. H. Chen, Z. Q. Feng, J. Q. Li, and H. F. Zhang, Production of proton-rich nuclei around $Z = 84$–90 in fusion-evaporation reactions, Eur. Phys. J. A **53**, 95 (2017).

[51] W. Nörenberg, Quantum-statistical approach to gross properties of peripheral collisions between heavy nuclei, Z. Phys. A **274**, 241 (1975).

[52] P. Möller, A. J. Sierka, T. Ichikawa, and H. Sagawa, Nuclear ground-state masses and deformations: FRDM (2012), At. Data Nucl. Data Tables **109-110**, 1 (2016).

[53] P. H. Chen, Z. Q. Feng, J. Q. Li, and H. F. Zhang, A statistical approach to describe highly excited heavy and superheavy nuclei, Chin. Phys. C **40**, 091002 (2016).

[54] Z. Q. Feng, G. M. Jin, F. Fu, and J. Q. Li, Production cross sections of superheavy nuclei based on dinuclear system model, Nucl. Phys. A **771**, 50 (2006); Z. Q. Feng, G. M. Jin, J. Q. Li, and W. Scheid, Formation of superheavy nuclei in cold fusion reactions, *ibid.* **76**, 044606 (2007).

[55] M. G. Itkis, J. Aysto, S. Beghini *et al.*, Shell effects in fission and quasi-fission of heavy and superheavy nuclei, Nucl. Phys. A **734**, 136 (2004).

[56] V. Zagrebaev and W. Greiner, Unified consideration of deep inelastic, quasi-fission and fusion-fission phenomena, J. Phys. G: Nucl. Part. Phys. **31**, 825 (2005).

[57] Yu. Ts. Oganessian, V. K. Utyonkov, Y. V. Lobanov, F. S. Abdullin, A. N. Polyakov, I. V. Shirokovsky *et al.*, Measurements of cross sections and decay properties of the isotopes of elements 112, 114, and 116 produced in the fusion reactions ^{233,238}U, ^{242}Pu, and ^{248}Cm + ^{48}Ca, Phys. Rev. C **70**, 064609 (2004).

[58] Z. Cheng and X. J. Bao, Formation of heavy neutron-rich nuclei by ^{48}Ca-induced multinucleon transfer reactions, Phys. Rev. C **103**, 024613 (2021).

[59] L. G. Moretto and R. P. Schmitt, Deep inelastic reactions: A probe of the collective properties of nuclear matter, Rep. Prog. Phys. **44**, 533 (1981).

[60] V. E. Viola, Nucleus-nucleus collisions: A laboratory for studying equilibration phenomena, Acc. Chem. Res. **20**, 32 (1987).

[61] C. Simenel, K. Godbey, and A. S. Umar, Timescales of Quantum Equilibration, Dissipation and Fluctuation in Nuclear Collisions, Phys. Rev. Lett. **124**, 212504 (2020).